Heat and Mass Transfer 37 (2001) 299–308 © Springer-Verlag 2001

Hydrodynamic and heat transfer characteristics of laminar flow past a parabolic cylinder with constant heat flux

M. Abu-Qudais, O. M. Haddad, A. M. Maqableh

Abstract Steady, two-dimensional, symmetric, laminar and incompressible flow past parabolic bodies in a uniform stream with constant heat flux is investigated numerically. The full Navier–Stokes and energy equations in parabolic coordinates with stream function, vorticity and temperature as dependent variables were solved. These equations were solved using a second order accurate finite difference scheme on a non-uniform grid. The leading edge region was part of the solution domain. Wide range of Reynolds number (based on the nose radius of curvature) was covered for different values of Prandtl number. The flow past a semi-infinite flat plate was obtained when Reynolds number is set equal to zero. Results are presented for pressure and temperature distributions. Also local and average skin friction and Nusselt number distributions are presented. The effect of both Reynolds number and Prandtl number on the local and average Nusselt number is also presented.

List of symbols

C_f	skin friction coefficient
D	dimensionless length
f	scaled non-dimensional stream function
g	scaled non-dimensional vorticity
h	scaled non-dimensional temperature
h_o	convection heat transfer coefficient
i	numerical index in streamwise direction
i_{buf}	the index i at the beginning of the buffer zone
j	numerical index in the wall normal direction
k	the thermal conductivity
m	total band width of a banded matrix
Nu	Nusselt number ($\mathrm{Nu} = h\xi_{max}/k$)
n	the order of a banded matrix
P	scaled non-dimensional pressure
p	the non-dimensional pressure
Pr	Prandtl number ($\mathrm{Pr} = \nu/\alpha$)
q	heat flux per unit area
R	the nose radius of curvature of the parabola
Re	Reynolds number based on the nose radius of curvature $\mathrm{Re} = U_\infty R/\nu$)
r	the radius of curvature of the parabola
s	weighting factor
T_w	wall temperature
T_∞	free stream temperature
U_∞	free-stream velocity
(x, y)	the Cartesian coordinates system
(ξ, η)	the parabolic coordinates system

Greek symbols

α	the thermal diffusivity
θ	non-dimensional temperature
ν	the kinematics viscosity
μ	dynamic viscosity
ψ	stream function
ω	vorticity
ϕ	viscous dissipation

1 Introduction

Some of the simplest flow problems such as flow past parabolas, wedges, flat plates, paraboloids and cones are of great importance and yet have received little attention [1]. In particular, the flow past a parabola is of practical interest in Aerospace since aerodynamic bodies designed for subsonic flow generally have finite thickness distributions with a parabolic leading edge [2]. Also, in turbomachinery applications, the cross-section of the blades is usually identical with those of the airfoils.

All previous investigations in the literature [1, 3–6] presented solutions only for the Navier–Stokes equations that govern the hydrodynamic part of the problem. The goal of this study is to solve the energy equation in addition to Navier–Stokes equations, and thus to present the local and average skin friction distributions as well as the local and average Nusselt number distributions for different values of the flow parameters, e.g. Re, Pr. Furthermore, the flow past a semi-infinite flat plate can be obtained as a special case of flow past a parabolic body as the Reynolds number, based on the nose radius of curvature, is set equal to zero.

Davis [5] used parabolic coordinates to solve the laminar incompressible flow past a semi-infinite flat plate using truncation series or local similarity method applied on full Navier–Stokes equations. The difficulty of matching approximation of low Reynolds number (Stokes) approxi-

Received on 5 July 2000

M. Abu-Qudais (✉), O. M. Haddad
Jordan University of Science and Technology
Department of Mechanical Engineering
P.O. Box 3030, Irbid 22110, Jordan

A. M. Maqableh
Al-Balqa Applied University Al-Huson Polytechnic
P.O. Box 50, Huson 21510, Jordan

mation with high Reynolds number (boundary layer) approximation is avoided and the solution is obtained for all values of Reynolds number. Van De Vooren and Dijkstra [7] applied the same approach used by Davis [5] to solve numerically the nature of the flow near the leading edge of flat plate. They used simple finite difference expressions and the system of equations was solved by iterative technique. Their solution was also valid for any value of Reynolds number. They have shown that there is about 5% error in the results of Davis [5] near the leading edge in skin friction.

The flow over a parabolic cylinder has been numerically studied by Davis [1]. An alternating direction implicit method was used to solve the time dependent Navier–Stokes equations. Careful attention was focused by Davis on extracting the singularities from the problem in the limit as Reynolds number goes to zero (flat plate). The same flow problem was treated by Dennis and Walsh [4] using finite difference approximations to the partial differential equations for the stream function and vorticity as dependent variables. In their study, Dennis and Walsh were not able to get a solution for Reynolds number smaller than 0.25 because of singularity problem, although their results were in good agreement with those of Davis [1]. They had a small but significant difference between their results and those of the second order boundary layer approximation especially in skin friction.

The method of solution of Van De Vooren and Dijkstra [7] for the semi-infinite flat plate was extended to the case of parabolic cylinder by Botta, Dijkstra and Veldman [6]. They managed to extend the solution for the case of Reynolds number approaches infinity (boundary layer). The drag coefficient have been checked by means of application of the momentum theory to an infinitely large circular contour and the deviation was within 2% for smallest mesh size.

Finally, the results of this study are presented for pressure, velocity and temperature distributions in addition to local and average skin friction and Nusselt number distributions and then compared with the case of Isothermal wall temperature case [8].

2 Analysis

The schematic diagram in Fig. 1 shows the flow problem under consideration. The equation of the surface of the parabolic body is given by

$$x(y) = \frac{1}{2R}(y^2 - R^2) \tag{1}$$

where R is recognized as the nose radius of curvature.

2.1 Governing equations

The full dimensional Navier–Stokes (N–S) and energy equations for two dimension, laminar, steady, viscous and incompressible fluid flow in Cartesian coordinates for stream function (ψ^*), vorticity (ω^*) and temperature (T^*) variables are given by:

Stream function equation:

$$\frac{\partial^2\psi^*}{\partial x^{*2}} + \frac{\partial^2\psi^*}{\partial y^{*2}} = -\omega^* \tag{2}$$

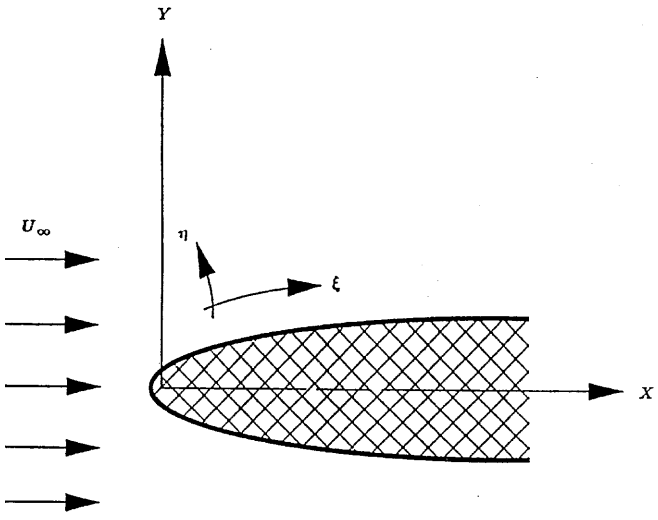

Fig. 1. Schematic diagram for parabolic body in symmetric mean flow

Vorticity equation:

$$\frac{\partial\psi^*}{\partial y^*}\frac{\partial\omega^*}{\partial x^*} - \frac{\partial\psi^*}{\partial x^*}\frac{\partial\omega^*}{\partial y^*} = \nu\left(\frac{\partial^2\omega^*}{\partial x^{*2}} + \frac{\partial^2\omega^*}{\partial y^{*2}}\right) \tag{3}$$

Energy equation:

$$\frac{\partial\psi^*}{\partial y^*}\frac{\partial T^*}{\partial x^*} - \frac{\partial\psi^*}{\partial x^*}\frac{\partial T^*}{\partial y^*} = \alpha\left(\frac{\partial^2 T^*}{\partial x^{*2}} + \frac{\partial^2 T^*}{\partial y^{*2}}\right) \tag{4}$$

where the velocity is related to the stream function by

$$u^* = \frac{\partial\psi^*}{\partial y^*} \quad \text{and} \quad v^* = -\frac{\partial\psi^*}{\partial x^*}$$

and the vorticity is defined as

$$\omega^* = \frac{\partial v^*}{\partial x^*} - \frac{\partial u^*}{\partial y^*}$$

where it is assumed that there is no heat source/sink, the thermophysical properties are constant, and the viscous dissipation is negligible. The following dimensionless variables are introduced to change the above governing equations into a non-dimensional form

$$x = \frac{x^*}{(\upsilon/U_\infty)}, \quad y = \frac{y^*}{(\upsilon/U_\infty)}, \quad \omega = \frac{\omega^*}{(U_\infty^2/\upsilon)},$$

$$\psi = \frac{\psi^*}{\upsilon}, \quad \theta = \frac{T^* - T_\infty^*}{T_w^* - T_\infty^*} \quad \text{and} \quad q = \frac{q^*\upsilon}{kU_\infty\Delta T^*}$$

substituting these variables into Eqs. (2, 3 and 4) yields the following dimensionless form of the equations

$$\psi_{xx} + \psi_{yy} = -\omega \tag{5}$$

$$\psi_y\omega_x - \psi_x\omega_y = \omega_{xx} + \omega_{yy} \tag{6}$$

$$\psi_y\theta_x - \psi_x\theta_y = \frac{1}{\mathrm{Pr}}(\theta_{xx} + \theta_{yy}) \tag{7}$$

where subscripts denote partial differentiation and Pr is the Prandtl number.

For this particular flow problem, a body fitted (parabolic) coordinates (ξ, η) can be used. These are related to

the dimensionless Cartesian coordinates (x, y) by the complex equation:

$$(x + \mathrm{i}y) = \frac{(\xi + \mathrm{i}\eta)^2}{2}$$

or

$$x = \frac{\xi^2 - \eta^2}{2}, \quad y = \xi\eta \tag{8}$$

thus, Eqs. (5, 6 and 7) can be rewritten in parabolic variables as

$$\psi_{\xi\xi} + \psi_{\eta\eta} = -(\xi^2 + \eta^2)\omega \tag{9}$$

$$\left[\frac{\partial^2}{\partial\xi^2} + \frac{\partial^2}{\partial\eta^2} + \frac{\partial\psi}{\partial\xi}\frac{\partial}{\partial\eta} - \frac{\partial\psi}{\partial\eta}\frac{\partial}{\partial\xi}\right]\omega = 0 \tag{10}$$

$$\left[\frac{1}{\mathrm{Pr}}\left(\frac{\partial^2}{\partial\xi^2} + \frac{\partial^2}{\partial\eta^2}\right) + \frac{\partial\psi}{\partial\xi}\frac{\partial}{\partial\eta} - \frac{\partial\psi}{\partial\eta}\frac{\partial}{\partial\xi}\right]\theta = 0 \tag{11}$$

To remove the singularity at the leading edge of the flat plate, we follow Davis [1] and introduce the new variables f, g, and h which are related to ψ, ω and θ by

$$\psi = \xi f(\xi, \eta), \quad \omega = -\frac{\xi}{(\xi^2 + \eta^2)}g(\xi, \eta)$$

and

$$\theta = -\frac{\xi}{(\xi^2 + \eta^2)}h(\xi, \eta) \tag{12}$$

substituting Eq. (12) back into Eqs. (9–11), one can get the following equations that govern the new dependent variables *f*, *g*, and *h*

$$f_{\eta\eta} - g + \left(f_{\xi\xi} + \frac{2}{\xi}f_\xi\right) = 0 \tag{13}$$

$$\begin{aligned} &g_{\eta\eta} + \left(f + \xi f_\xi - \frac{4\eta}{\xi^2 + \eta^2}\right)g_\eta \\ &\quad + \left(\frac{\xi^2 - \eta^2}{\xi^2 + \eta^2}f_\eta - \frac{2\eta}{\xi^2 + \eta^2}(f + \xi f_\xi)\right)g \\ &\quad - \xi g_\xi\left(f_\eta + \frac{4\xi}{\xi^2 + \eta^2}\right) + \left(g_{\xi\xi} + \frac{2}{\xi}g_\xi\right) = 0 \end{aligned} \tag{14}$$

$$\begin{aligned} &h_{\eta\eta} + \left(\mathrm{Pr}(f + \xi f_\xi) - \frac{4\eta}{\xi^2 + \eta^2}\right)h_\eta \\ &\quad + \mathrm{Pr}\left(\frac{\xi^2 - \eta^2}{\xi^2 + \eta^2}f_\eta - \frac{2\eta}{\xi^2 + \eta^2}(f + \xi f_\xi)\right)h \\ &\quad - \xi h_\xi\left(\mathrm{Pr}\, f_\eta + \frac{4\xi}{\xi^2 + \eta^2}\right) + \left(h_{\xi\xi} + \frac{2}{\xi}h_\xi\right) = 0 \end{aligned} \tag{15}$$

The above equations form a system of non-linear and elliptic partial differential equations. The equations are parabolic in ξ if the last two terms in each equation are neglected. This fact is exploited in the numerical solution of Davis [1].

2.2 Boundary conditions

Using Eq. (8), one can find that

$$\eta = \sqrt{\xi^2 - 2x}$$

therefore at the leading edge of the parabola where $\xi = 0, \eta$ is given by

$$\eta_{\mathrm{LE}} = \sqrt{-2x}$$

however, from Eq. (1)

$$x_{\mathrm{LE}} = x(y = 0) = -R/2$$

thus,

$$\eta_{\mathrm{LE}} = \sqrt{-2\frac{-R}{2}} = R^{1/2}$$

therefore, because η at the surface of the parabolic body is constant, the wall of the parabola is located at:

$$\eta_{\mathrm{w}} = \eta_{\mathrm{LE}} = R^{1/2}$$

since we use a viscous length scale, R can also be interpreted as the Reynolds number based on the nose radius of curvature (R in its dimensional form is the nose radius of curvature; but when non-dimensionalized, it is Reynolds number based on the nose radius of curvature).

The boundary conditions of the problem under consideration can be expressed as follows:
At the wall $(\eta = \mathrm{Re}^{1/2})$:
the no-slip $(u = 0)$, no penetration $(v = 0)$ conditions at the surface require that

$$\psi|_{\mathrm{wall}} = \text{constant} = 0 \quad \text{and} \quad \frac{\partial\psi}{\partial\eta}|_{\mathrm{wall}} = 0$$

or

$$f = 0 \quad \text{and} \quad \frac{\partial f}{\partial\eta} = 0 \tag{16}$$

where

$$u = \frac{\partial\psi}{\partial y} = \left[\frac{\partial\psi}{\partial\xi}\frac{\partial\xi}{\partial y} + \frac{\partial\psi}{\partial\eta}\frac{\partial\eta}{\partial y}\right]$$

$$v = -\frac{\partial\psi}{\partial x} = -\left[\frac{\partial\psi}{\partial\xi}\frac{\partial\xi}{\partial x} + \frac{\partial\psi}{\partial\eta}\frac{\partial\eta}{\partial x}\right]$$

By applying the stream function Eq. (9) at the wall with $(\psi_\xi = \psi_{\xi\xi} = \psi_\eta = 0)$, the vorticity condition is then given by

$$\omega|_{\mathrm{wall}} = \frac{-1}{(\xi^2 + \eta^2)}\psi_{\eta\eta}$$

and in terms of g using Eq. (12)

$$g|_{\mathrm{wall}} = f_{\eta\eta} \tag{17}$$

and assuming constant heat flux at the wall, then

$$-k\left.\frac{\partial T^*}{\partial y^*}\right|_{\mathrm{w}} = q^*_{\mathrm{w}}$$

The above equation can be written in dimensionless form as:

$$\frac{\partial\theta}{\partial y} = -q_{\mathrm{w}}$$

the above equation can be written in parabolic coordinates and in terms of (h) using Eqs. (8 and 12):

$$h^{\eta}\left(3\xi^2-\eta^2\right)-\xi\left(\xi^2+\eta^2\right)\left(\xi h_{\eta}+\eta h_{\xi}\right) = -q\left(\xi^2+\eta^2\right)^3 \tag{18}$$

At free-stream ($\eta \to \infty$) far away from the surface of the parabola in the wall normal direction, the flow is potential flow where $u^*_{\infty} = U_{\infty}$. Thus,

$$\psi|_{\eta\to\infty} \to \psi_{\infty}$$

but

$$u_{\infty} = 1 = \frac{\partial \psi_{\infty}}{\partial y}$$

therefore,

$$\psi_{\infty} \sim y \equiv \xi\eta$$

The stream-function condition can be rewritten in terms of f in the form

$$\frac{\partial f}{\partial \eta}|_{\eta\to\infty} \to 1 \tag{19}$$

The free-stream is vortex free because it is free of all velocity gradients $\left[\frac{\partial v}{\partial x}=\frac{\partial u}{\partial y}=0\right]$, thus the velocity condition is:

$$\omega|_{\eta\to\infty} \to 0$$

i.e

$$g|_{\eta\to\infty} \to 0 \tag{20}$$

Assuming the free-stream temperature is constant, then temperature condition is:

$$\theta|_{\eta\to\infty} \to 0$$
$$h|_{\eta\to\infty} \to 0 \tag{21}$$

Equations (13–15) with their boundary conditions form a system of steady non-linear partial differential equations that governs the flow problem at hand. Equations (13 and 14) are coupled in f and g and thus their solution can be used to solve Eq. (15) for h.

3 Numerical solution

The system of governing Eqs. (13–15) with their boundary conditions have been finite differenced on a non-uniform grid. The equations are also linearized using Newton's linearization technique [9]. The linearized equations were solved using the proper LINPACK [10] subroutines in double precision. Since Eq. (13 and 14) are similar to the equations solved by Haddad and Corke [3] and because the energy equation, Eq. (15), is mathematically similar to Eq. (14), this encouraged us to use the same approach used before by Haddad and Corke [3].

The computational grid in the physical plane is shown in Fig. 2. The computational grid in the numerical domain is shown in Fig. 3. In Fig. 3 the surface of the parabola is represented by the mesh line $\eta = \eta_w = \mathrm{Re}^{1/2}$ and the free stream is represented by the line $\eta = \eta_{max}$. The lower and upper regions of the flow in the physical plane are located

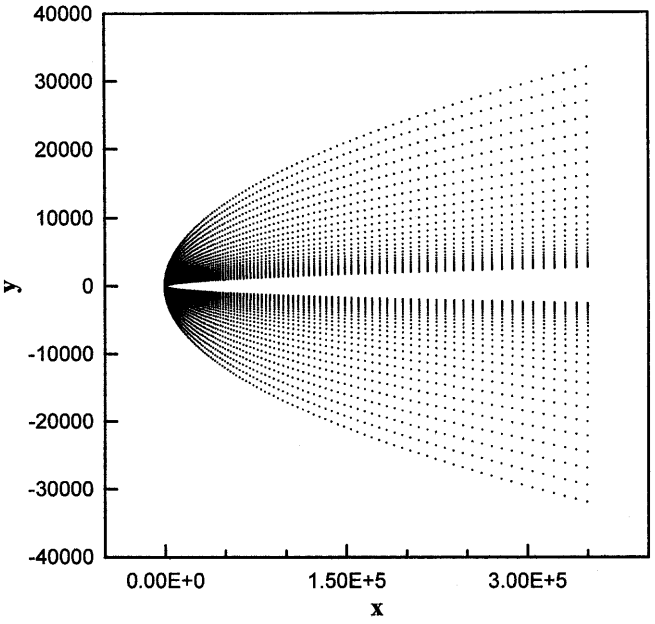

Fig. 2. The computational grid in physical plane; Re = 10

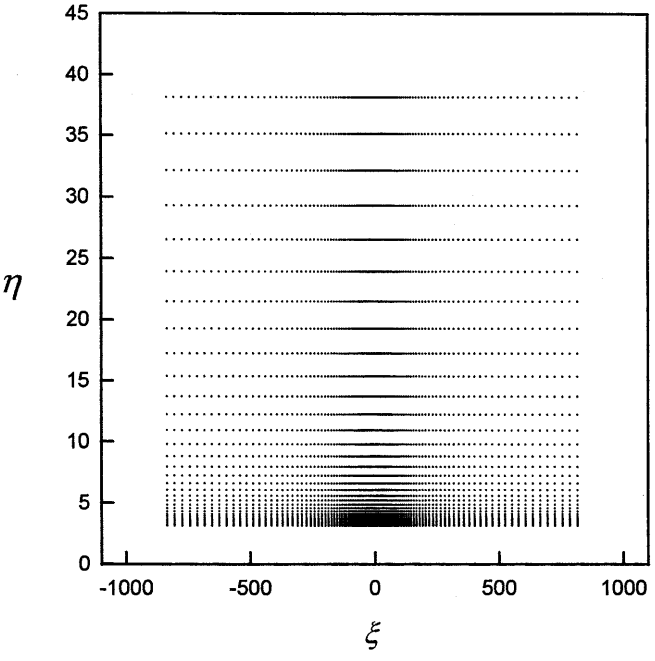

Fig. 3. The computational grid numerical plane; Re = 10

respectively between $-\xi_{max} \le \xi \le 0$ and $0 \le \xi \le \xi_{max}$ in the numerical plane.

Based on the study made by Haddad and Corke [3] and on the capacity of the computer facility available for this study, the far downstream (outflow) boundary was chosen at $x_{max} = 3.5 \times 10^5$. In the wall normal direction the wall is located at $\eta_w = \sqrt{\mathrm{Re}}$ and the freestream was chosen at $\eta = \eta_{max}$ where $\eta_{max} - \eta_w = 35$. This corresponds to a freestream boundary that is located at a distance normal to the wall which is 10-times the Blasius boundary layer thickness far downstream on a flat plate [3].

Boundary layer flows are characterized by having large gradient of flow quantities near the wall in the wall normal direction and near the leading edge in the flow direction. To treat this, more grid points have to be clustered at these locations. This was accomplished by using Robert's stretching transformation of the original uniform grid which has the form [9]

$$y = h\frac{(\beta+1)-(\beta-1)\{[(\beta+1)/(\beta-1)]^{1-\bar{y}}\}}{[(\beta+1)/(\beta-1)]^{1-\bar{y}}+1}$$

where $(\bar{x},\bar{y})$ represent the uniform grid plane, (x,y) are the stretched grid plane, β is the stretching parameter (constant) and h is the grid width in the direction in which the grid is being stretched.

The above transformation has been applied in both streamwise and wall normal directions. The stretching parameter β was chosen equal to 1.01 in ξ-direction and 1.005 in η-direction since these values gave convenient grid points spacing.

Before solving the governing equations, Eqs. (13–15) with their boundary conditions, Newton's linearization technique [9] was applied to linearize the governing equations.

To implement the boundary conditions at downstream infinity, a buffer-zone was specified in which the elliptic terms in the governing equations have been multiplied by a weighting factor, s. The weighting factor was a function of streamwise location only. At the beginning of the buffer zone, $s=1$. At the end of the buffer zone, which corresponds to the outflow boundary, $s=0$. For smooth transition from 1 to 0, the weighting factor was given the following form

$$s(i) = \frac{1+\tanh(\arg)}{2}$$

where

$$\arg = 4\left[1-\frac{2(i-i\text{buf})}{(I_{\max}-i\text{buf})}\right]$$

where i is the numerical index in the streamwise direction and $i$buf is the index i at the beginning of the buffer-zone [3]. After applying Newton's linearization technique and multiplying the elliptic terms by the weighting factor $s(i)$, the governing Eqs. (13–15) at every new iteration $(n+1)$ take the form:

$$f_{\eta\eta}^{n+1} - g^{n+1} + s(i)\left[f_{\xi\xi\xi}^{n+1} + \frac{2}{\xi}g_{\xi}^{n+1}\right] = 0 \tag{22}$$

$$\begin{aligned}
&g_{\eta\eta}^{n+1} + \left[f^n g_n^{n+1} + f^{n+1}g_\eta^n - f^n g_\eta^n\right] \\
&\quad + \xi\left[f_\xi^n g_\eta^{n+1} + f_\xi^{n+1}g_\eta^n - f_\xi^n g_\eta^n\right] \\
&\quad - \frac{4\eta}{\xi^2+\eta^2}g_\eta^{n+1} + \frac{\xi^2-\eta^2}{\xi^2+\eta^2}\left[f_\eta^n g^{n+1} + f_\eta^{n+1}g^n - f_\eta^n g^n\right] \\
&\quad - \frac{4\xi}{\xi^2+\eta^2}g_\xi^{n+1} - \frac{2\eta}{\xi^2+\eta^2}\left[f^n g^{n+1} + f^{n+1}g^n - f^n g^n\right] \\
&\quad - \frac{2\xi\eta}{\xi^2+\eta^2}\left[f_\xi^n g^{n+1} + f_\xi^{n+1}g^n - f_\xi^n g^n\right] \\
&\quad - \xi\left[f_\eta^n g_\xi^{n+1} + f_\eta^{n+1}g_\xi^n - f_\eta^n g_\xi^n\right] \\
&\quad + s(i)\left[g_{\xi\xi\xi}^{n+1} + \frac{2}{\xi}g_\xi^{n+1}\right] = 0
\end{aligned} \tag{23}$$

$$\begin{aligned}
&h_{\eta\eta}^{n+1} + \mathrm{Pr}\left[f^n h_\eta^{n+1} + f^{n+1}h_\eta^n - f^n h_\eta^n\right] \\
&\quad + \xi\ \mathrm{Pr}\left[f_\xi^n h_\eta^{n+1} + f_\xi^{n+1}h_\eta^n - f_\xi^n h_\eta^n\right] \\
&\quad - \frac{4\eta}{\xi^2+\eta^2}h_\eta^{n+1} + \frac{\xi^2-\eta^2}{\xi^2+\eta^2}\mathrm{Pr}\left[f_\eta^n h^{n+1} + f_\eta^{n+1}h^n - f_\eta^n h^n\right] \\
&\quad - \frac{4\xi}{\xi^2+\eta^2}h_\xi^{n+1} - \frac{2\eta}{\xi^2+\eta^2}\mathrm{Pr}\left[f^n h^{n+1} + f^{n+1}h^n - f^n h^n\right] \\
&\quad - \frac{2\xi\eta}{\xi^2+\eta^2}\mathrm{Pr}\left[f_\xi^n h^{n+1} + f_\xi^{n+1}h^n - f_\xi^n h^n\right] \\
&\quad - \xi\ \mathrm{Pr}\left[f_\eta^n h_\xi^{n+1} + f_\eta^{n+1}h_\xi^n - f_\eta^n h_\xi^n\right] \\
&\quad + s(i)\left[h_{\xi\xi\xi}^{n+1} + \frac{2}{\xi}h_\xi\right] = 0
\end{aligned} \tag{24}$$

The above system of governing equations have been discretized using the same difference scheme used by Haddad and Corke [3]. A second order accurate finite difference scheme on a non-uniform grid was used.

Upon the above strategy, there are always 3-points involved in the difference equations in both ξ and η directions at any grid point. The only exception to that is at the outflow boundaries. At the outflow boundaries, we chose to involve only one point in difference equations in the streamwise direction. This was done to reduce the bandwidth of the coefficient matrix to half its value in the case when two points are involved at the outflow.

Starting with an initial guess, iteration was carried out until the maximum absolute local error is less than 10^{-5}. Here the local error is defined as the difference in the local solution between the new iteration $(n+1)$ and old iteration (n).

Finally, LINPACK subroutines [10] (standard linear algebraic equations solver package) have been used to solve the resulting system of linear algebraic equations with double precision arithmetic in all calculations. All programs and subroutines were written in Fortran77. The computer used for this study was the digital alpha machine based on UNIX operating system]. Generally, it took about seven iterations or equivalently one and half an hour of real computer time to achieve convergence for most of the cases studied here.

4 Results and discussion

A numerical code has been written to provide solutions for the Navies–Stokes equations and energy equation. The results of this code will be presented and discussed. Numerical test calculations were carried out by Haddad and Corke [3] to evaluate the effect of downstream boundary location, freestream boundary location, grid size (number of grid points) and grid spacing (stretching in both streamwise and wall normal direction) on the solution. In investigating the effect of each of the above parameters,

only one parameter was varied at a time, and the attention was focused on the wall vorticity to judge the solution sensitivity to the changing parameter. The detailed results can be found by referring to Haddad, Abu-Qudais and Maqableh [8].

A sample result of the grid sensitivity study is shown in Fig. 4. Since flow past a parabola is known to approach the flat plate Blasius flow, the vorticity at the wall should be invariant with the streamwise location far downstream. Two curves in Fig. 4 show a trend which is definitely wrong. The grid size corresponds to these cases was 350×28 and 200×30. The other cases show the proper asymptotic behavior which agrees with the Blasius flow. Figure 4 shows that the numerical results are more sensitive to the number of grid points in the wall normal direction ($J_{\max}$) than in the streamwise direction ($I_{\max}$). Almost identical results were obtained for the cases with $I_{\max} = 150$ and $I_{\max} = 350$ whereas significant change in the solution have occurred when $J_{\max}$ is changed from 30 to 33. The solid curve in figure corresponds to the grid size 200×36 points which was used throughout this study.

4.2 Hydrodynamic field

In this section pressure distribution along the parabolic surface, local and average skin friction distributions and velocity profiles normal to the wall at different streamwise locations are presented and discussed.

The effect of bluntness (i.e. Reynolds number based on the nose radius of curvature) on the surface pressure distribution is determined. To validate our approach, results of this study are compared with the solutions obtained by Haddad et al. [8].

To find an expression for the surface pressure distribution, we start with the dimensional x^*-momentum equation in the form

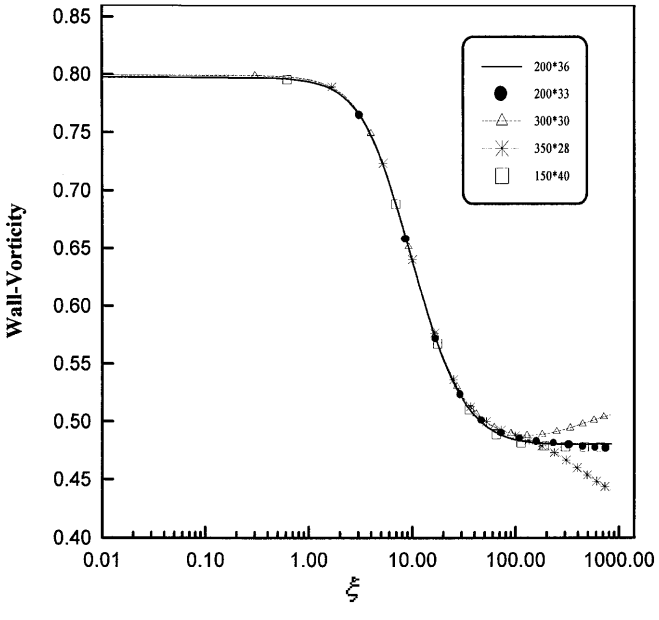

Fig. 4. Effect of grid size on vorticity along a parabolic cylinder; $\mathrm{Re} = 10$

$$u^* \frac{\partial u^*}{\partial x^*} + v^* \frac{\partial u^*}{\partial y^*} = -\frac{1}{\rho}\frac{\partial p^*}{\partial x^*} + \nu\left[\frac{\partial^2 u^*}{\partial x^{*2}} + \frac{\partial^2 u^*}{\partial y^{*2}}\right]$$

applying the above equation at the wall where

$$u^* = v^* = 0, \quad \text{where } u^* = \frac{\partial \psi^*}{\partial y^*}$$

also, introducing the dimensionless pressure defined in the form

$$p = \left(p^* - p^*_{\xi \to -\infty}\right)/(\rho U_\infty^2)$$

and changing the independent variables (x, y) to the parabolic variables (ξ, η) by using Eq. (8) yields

$$\frac{\partial p}{\partial \xi} = -\frac{\partial \omega}{\partial \eta}$$

and by using Eq. (12)

$$\frac{\partial p}{\partial \xi} = \frac{\xi}{\xi^2 + \eta^2}\left[\frac{\partial g}{\partial \eta} - \frac{2\eta}{\xi^2 + \eta^2} g\right]$$

Now, to remove the singularity of the pressure at the leading edge of the flat plate, we follow Davis [1] and introduce

$$P = p - \frac{\eta}{\xi^2 + \eta^2} g(0, R^{1/2})$$

thus,

$$\frac{\partial P}{\partial \xi} = \frac{\xi}{\xi^2 + \eta^2}\left[\frac{\partial g}{\partial \eta} - \frac{2\eta}{\xi^2 + \eta^2}(g - g_o)\right]$$

where $g_o = g(0, \mathrm{Re}^{1/2})$. Integrating the above expression starting at downstream infinity on the lower surface, the local pressure distribution is then given by

$$P = \int_{-\xi_{\max}}^{\xi} \frac{Z}{Z^2 + \eta^2}\left[\frac{\partial g}{\partial \eta} - \frac{2\eta}{Z^2 + \eta^2}(g - g_o)\right] \mathrm{d}Z \qquad (25)$$

The above integration was carried out using the trapezoidal rule. Figure 5 shows the surface pressure distribution for different parabolas. The results are in excellent agreement with those of Davis [1]. Here the solution in the buffer zone is excluded because the elliptic terms are killed gradually in this zone. The pressure gradient everywhere is favorable. We also note that the distributions asymptote to the same value regardless of Reynolds number value, this is because the flow past a parabola approaches the flat plate Blasius flow downstream away from the leading edge.

The local skin friction coefficient is defined as

$$C_f = \frac{\tau_w^*}{\rho U_\infty^2}$$

where $\tau^* = \mu\, \partial u^*/\partial y^*$. Rewriting u^* in terms of ψ^*, and non-dimensionalizing the variables to get

$$C_f = \frac{\partial^2 \psi}{\partial y^2}\Big|_w$$

but upon applying the stream function equation at the wall

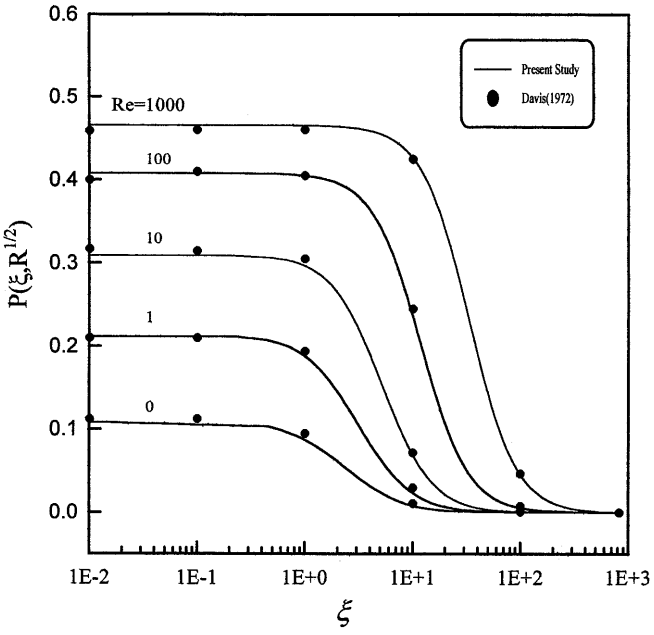

Fig. 5. Pressure distribution on parabolic bodies

$$\frac{\partial^2 \psi}{\partial y^2} = -\omega$$

therefore

$$C_f = -\omega|_w$$

finally, by using Eq. (12) the above equation becomes

$$C_f = \frac{\xi}{\xi^2 + \eta_w^2} g(\xi, R^{1/2}) \tag{26}$$

Figure 6 shows the scaled skin friction distribution $g(\xi, R^{1/2})$ for different parabolas. These distributions are qualitatively similar to the pressure distributions discussed previously. It can be noted that the more blunt the body, the larger is the local skin friction, with the maximum value being at the leading edge. However, all distributions asymptote to the same value far downstream from the leading edge as expected. Obviously, there is an excellent agreement between our results and those of Davis [1].

The average skin friction coefficient is defined as

$$\bar{C}_f = \frac{1}{\xi_{max}} \int_0^{\xi_{max}} C_f(\xi) d\xi$$

substituting for $C_f(\xi)$ using Eq. (26), then

$$\bar{C}_f = \frac{1}{\xi_{max}} \int_0^{\xi_{max}} \frac{\xi}{\xi^2 + \eta_w^2} g(\xi, R^{1/2}) d\xi$$

the above integration was evaluated using the trapezoidal rule. The average skin friction is defined as

$$\bar{g} = \frac{1}{\xi_{max}} \int_0^{\xi_{max}} g(\xi, R^{1/2}) d\xi \tag{27}$$

In Fig. 7 the result of the above integral is shown versus Reynolds number. It can be seen that the skin friction is minimum for the case Re = 0 (flat plate) and it increases gradually as the body becomes more blunt (i.e. as the Reynolds number based on the nose radius of curvature is increased). This can be attributed to the increase in both bluntness and surface area as Reynolds number is increased.

Anywhere in the flow field, the velocity can be calculated as

$$u^* = \frac{\partial \psi^*}{\partial y^*}$$

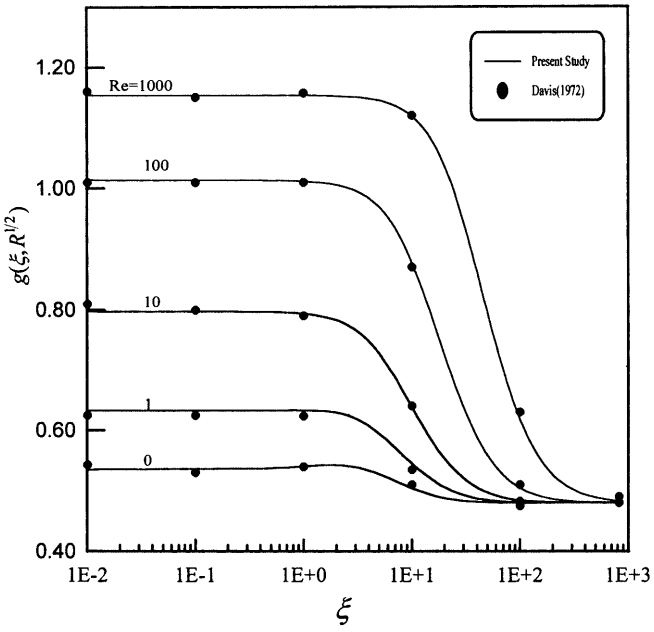

Fig. 6. Skin friction distribution on parabolic bodies

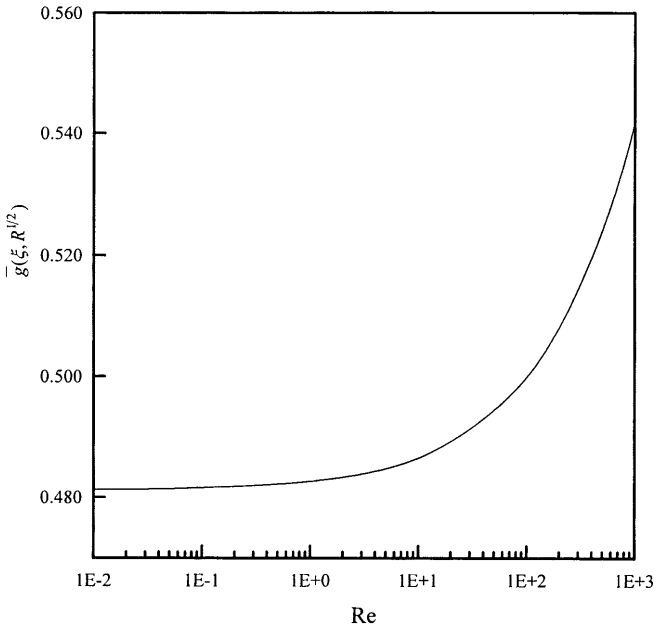

Fig. 7. Effect of Reynolds number on average skin friction

by non-dimensionalizing the variables and using Eqs. (8 and 12) the local velocity is then given as

$$u = \frac{\xi}{\xi^2 + \eta^2}\left[\xi\frac{\partial f}{\partial \eta} + \eta\frac{\partial f}{\partial \xi} + \frac{\eta}{\xi}f\right]$$

Numerical calculations were performed to compare the far downstream velocity profiles with the flat plate Blasius profile, and determine the streamwise velocity development inside the boundary layer at fixed height above the surface (i.e. fixed η-location). Figure 8 shows the hydrodynamic boundary layer thickness (the thickness at which $u = 0.99U_\infty$) for the case Re = 0 (flat plate). In the figure it is clearly seen that the boundary layer thickness increases as we go far downstream. In Fig. 9 the effect of Reynolds number on the downstream location at which the flow over parabolic body matches the Blasius flow is shown. As Reynolds number increases (more blunt body) the flow over parabolic body matches the Blasius profile farther downstream.

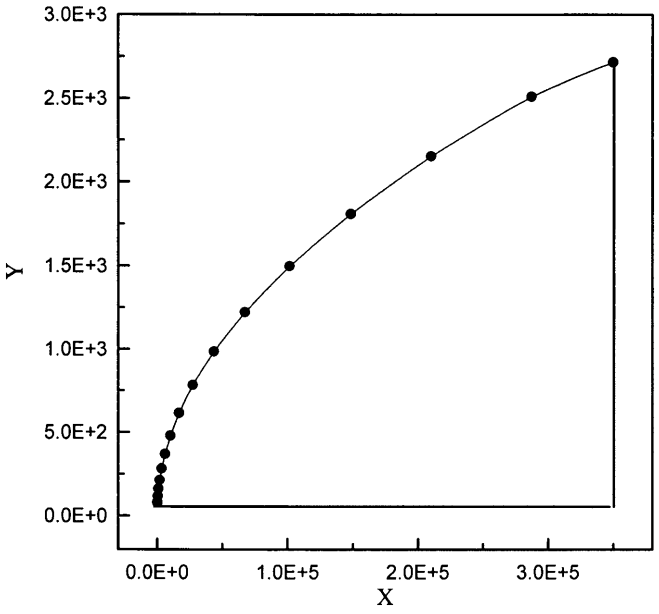

Fig. 8. Hydrodynamic boundary layer thickness; Re = 0 (Flat plate)

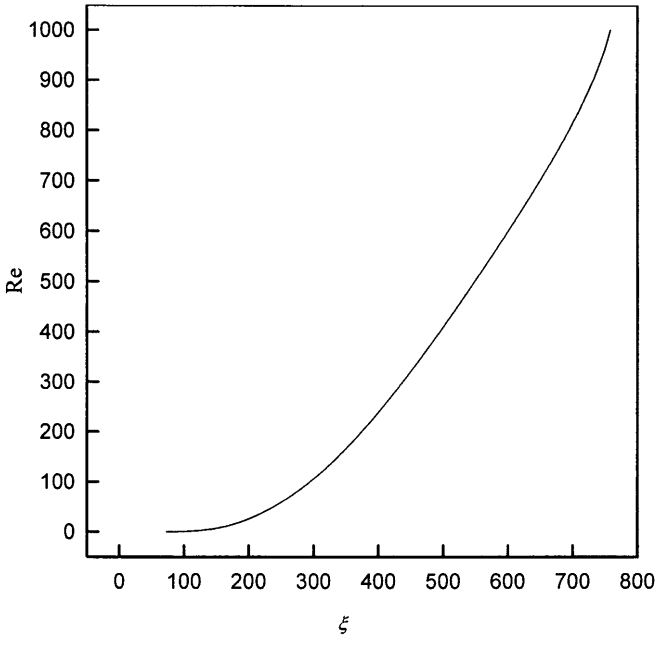

Fig. 9. Effect of Reynolds number on the streamwise direction at which flow over parabolic bodies approaches Blasius profile

4.3 Thermal field

The heat transfer between a parabolic surface and the flowing fluid over the surface with constant heat flux is considered. Numerical results for the temperature distri-

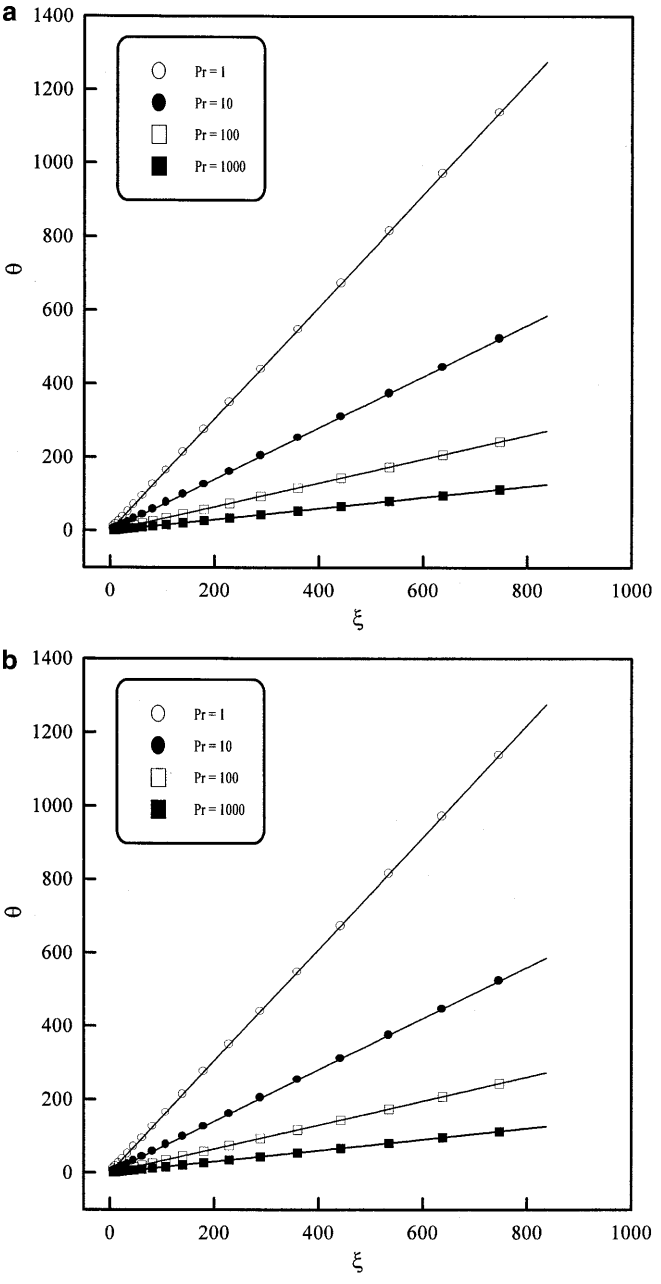

Fig. 10a, b. The streamwise temperature distribution at the wall ($j = 0$): **a** For Re = 0 (Flat plate); **b** for Re = 100 (Parabolic body)

bution and average mixing cup temperature distribution are presented. The effect of Prandtl number (Pr) and Reynolds number (Re) on Nusselt number (Nu) is also presented and discussed. Anywhere in the flow field, the local temperature can be calculated as

$$\theta(\xi,\eta) = -\frac{\xi}{\xi^2+\eta^2} h(\xi,\eta) \tag{28}$$

The surface temperature distributions for different values of Prandtl number for flat plate and parabolic body are shown in Fig. 10. It can be seen that as going along the surface away from the leading edge the temperature increases also as Prandtl number increases the temperature increases at the same streamwise location. Also there is no difference in the streamwise temperature distribution between the parabolic body and the flat plate. In other words, there is no effect for the bluntness of the body on the temperature distribution.

The average temperature distribution at the wall for different Prandtl number for flat plate and parabolic body has the same trend of the local temperature distribution as shown in Fig. 11. The only difference is that the magnitude of the local temperature is less than the average temperature at the same streamwise location and this is obviously seen in Fig. 12.

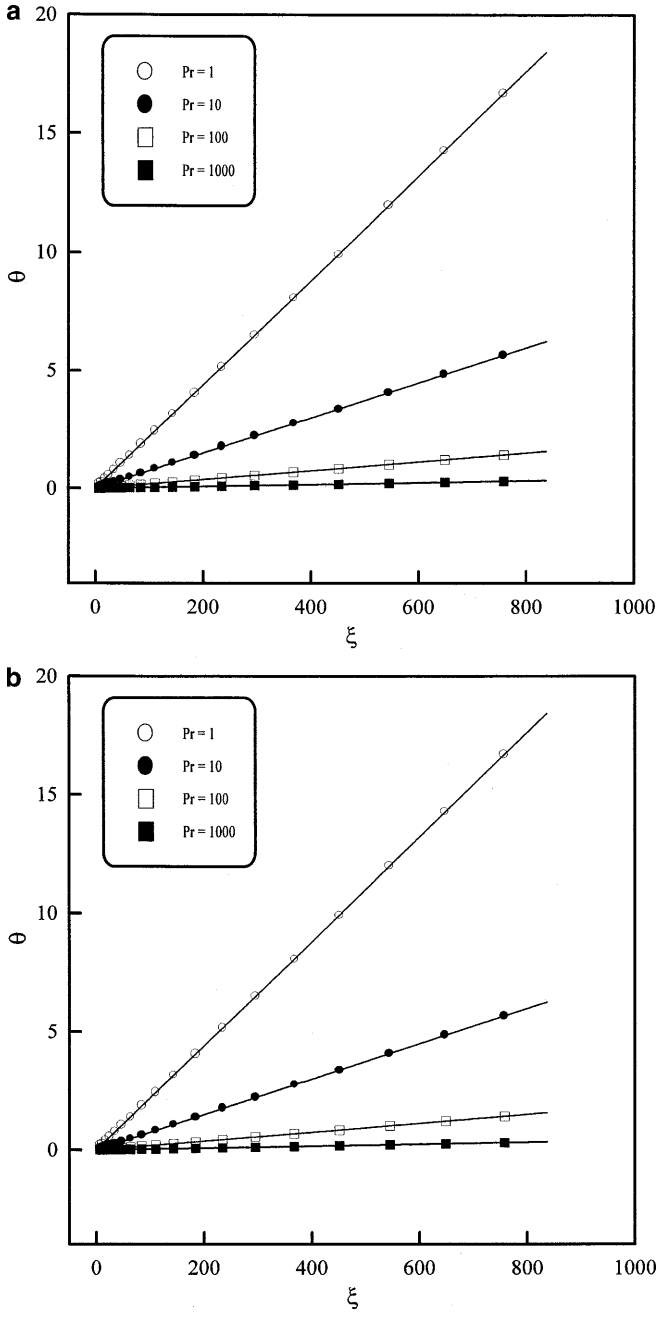

Fig. 11a, b. The Streamwise average temperature distribution at the wall: ($j = 0$): **a** For Re = 0 (Flat plate); **b** For Re = 100 (Parabolic body)

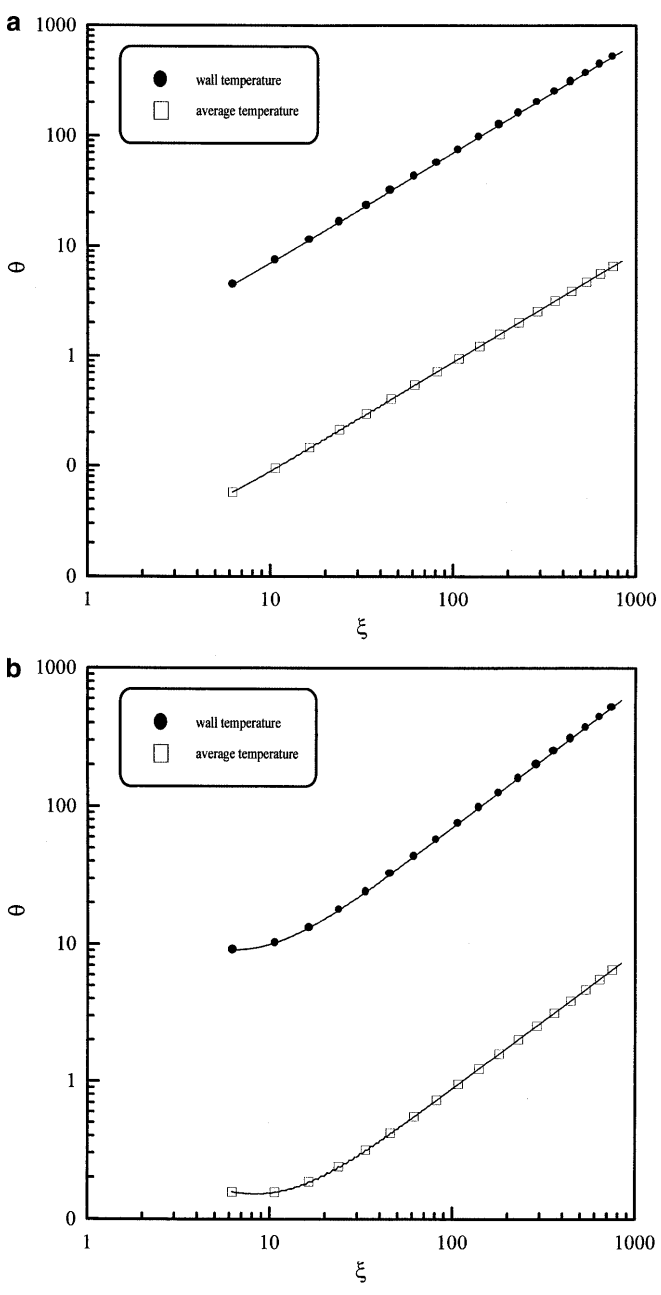

Fig. 12a, b. Comparison between the streamwise temperature distribution at the wall and the average temperature distribution at the wall ($j = 0$): **a** For Re = 0 (Flat plate); **b** for Re = 100 (Parabolic body), Pr = 10

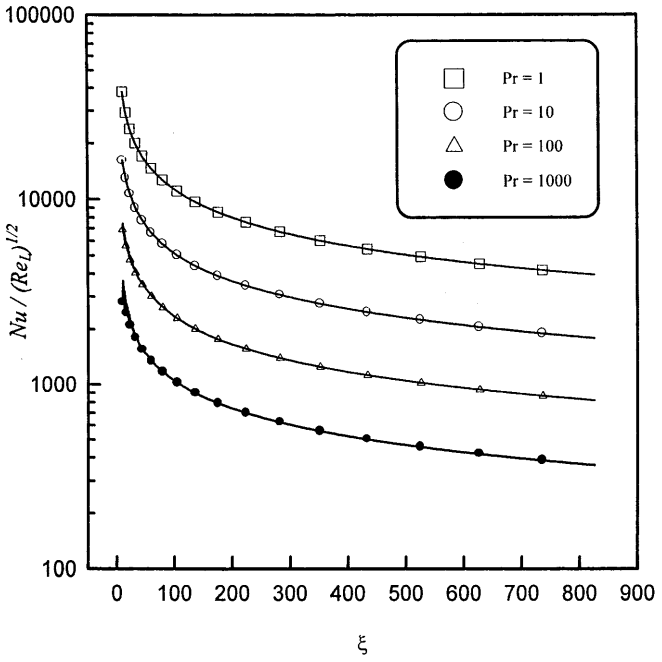

Fig. 13. Effect of Prandtl number on Nusselt number distribution for Re = 0 (Flat plate)

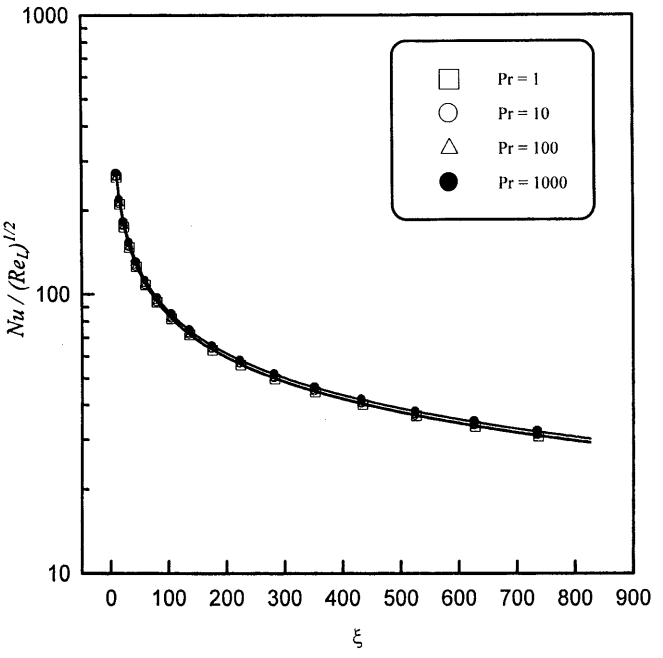

Fig. 14. Effect of Prandtl number on Nusselt number distribution for Re = 100 (Parabolic body)

Figure 13 shows the effect of streamwise location on Nusselt number distribution for flat plate (Re = 0) for different Prandtl number. Nusselt number decreases as we go far away from the leading edge and also as increasing Prandtl number. The effect of streamwise location on Nusselt number distribution for flow over parabolic body (Re = 100) for different Prandtl number is shown in Fig. 14. It is seen that Nusselt number decreases as we move far away from the leading edge. Most importantly, the effect of Prandtl number on Nusselt number distribution is negligible for the case of flow over parabolic body subjected to constant heat flux at the wall.

5 Conclusions

The hydrodynamic and thermal energy characteristics for laminar flow over parabolic body with constant heat flux were studied. The numerical codes allowed us to study the effect of both Reynolds number and Prandtl number on pressure, temperature, skin friction and Nusselt number distributions of flow over parabolic bodies with constant heat flux.

Both pressure and skin friction distribution increases as the parabolic body becomes more blunt (as Re increases). Both distributions take a maximum value at the leading edge and asymptote to downstream value away from the leading edge in the streamwise direction (where the Blasius flow holds). As a result, the average skin friction increases as Reynolds number increases.

For the flow over parabolic body, there is no effect of the bluntness of the parabolic body on the overall and local wall temperature. Also, as Prandtl number increases both the local and overall wall temperature decrease. Consequently, the average Nusselt number increases (insignificantly) as Prandtl Number increases.

References

1. **Davis RT** (1972) Numerical solution of Navier–Stokes equations for symmetric laminar incompressible flow past a parabola. J Fluid Mech 51: 417–433
2. **Hammerton PW; Kerschen EJ** (1996) Boundary layer receptivity for parabolic leading edge. J Fluid Mech 310: 243–267
3. **Haddad OM; Corke Th** (1998) Numerical study of leading edge receptivity over parabolic bodies. J Fluid Mech 368: 1–26
4. **Dennis SCR; Walsh JD** (1971) Numerical solution for steady symmetric flow past a parabolic cylinder in uniform stream flow. J Fluid Mech 50: 801–814
5. **Davis RT** (1967) Laminar incompressible flow past a semi-infinite flat plate. J Fluid Mech 27(3): 691–704
6. **Botta EFF; Dijkstra D; Veldman AEP** (1972) The numerical solution for Navier–Stokes equations for laminar incompressible flow past a parabolic cylinder. J Engg Mech 6(1): 63–81
7. **Van De Vooren AI; Dijkstra D** (1970) The Navier–Stokes solution for laminar flow past a semi-infinite flat plate. J Engg Math 4(1): 9–27
8. **Haddad OM; Abu-Qudais M; Maqableh AM (2000)** Numerical solutions of the Navier–Stokes and energy equations for laminar incompressible flow past a parabolic bodies. Int J Num Meth for Heat and Fluid Flow 10(1): 80–93
9. **Anderson DA; Tannehill JC; Pletcher RH** (1984) Computational Fluid Mechanics and Heat Transfer. Hemisphere Publishing Corp.
10. **Dongara JJ; Molar CB; Bunch JR; Stewart GW** (1979) LINPACK Users guide, Siam